MULTIVARIATE PEM/FT SPECTROMETRY: INTRINSIC DATA FUSION AND APPLICATIONS FOR IED AND CB DEFENSE

Tudor N. Buican*
Semiotic Engineering Associates LLC
Albuquerque, NM 87111

Arthur H. Carrieri
US Army RDECOM Edgewood Chemical Biological Center (ECBC)
Aberdeen Proving Ground, MD 21010

ABSTRACT

We present recent developments in the theory of a new class of active multivariate FT spectrometers and describe their potential uses in the optical detection and identification of improvised explosive devices (IEDs) and CB agents and contaminants. This technology is based on the use of dual ultra-high-speed (UHS) birefringence interferometers for the simultaneous and independent modulation of both illumination and collected beams, and employs photoelastic modulators (PEM) as the birefringent elements in these interferometers. With typical scan rates of 10^4–10^5 interferograms per second and broad spectral range, these instruments can rapidly collect multivariate spectral data describing, in a correlated way, the comprehensive excitation, emission, and delay/lifetime spectral properties of the sample/target. The intrinsic process of data fusion that melds the multivariate spectral data into one interferogram signal allows for the simultaneous and correlated use of all three spectral variables for improved discrimination and identification of chemical species of interest.

1. INTRODUCTION

PEM-based FT spectrometers can easily acquire 10^5 spectra (interferograms) per second and cover broad spectral ranges (UV to NIR with fused silica optics, and NIR to mid-IR with ZnSe optics). PEM-based interferometers can be used simultaneously to modulate both the illumination beam and the collected light. In such a system, the chirped modulation (Stann et al., 1996) of the illumination beam (Buican, 1993, 1995) encodes a time origin for each half-period of the PEM, as well as the spectrum of the illumination beam. The second PEM-based interferometer additionally encodes the spectrum of the collected light. The resulting interferogram represents a rich fusion of correlated data and presents the promise of improved detection, discrimination, and identification of chemical species through digital postprocessing.

We present in this paper a powerful and elegant mathematical interpretation of the linear mapping of multivariate PEM/FT spectrometry (M-PEMS). This interpretation exposes the way in which M-PEMS is a direct generalization of standard FT spectrometry by separating the complex effects sample (specific multivariate spectrum) and instrument (operating parameters and scanning characteristics) have on the interferogram. Furthermore, it sheds light on how an M-PEMS instrument should be designed and operated.

We further show that the separation into sample and instrument components leads to an understanding of M-PEMS systems as data fusion optical processors, and of how this important function can be externally controlled. This further opens the way to adaptive operation for improved spectral discrimination and identification of certain threats.

Finally, we discuss the strategic advantages offered by multivariate PEM/FT regarding (i) the protection of U. S. and Allied troops against IEDs and (ii) the early warning of dangerous environmental CB threats evolving in the open battlefield or in the homeland. The design and development of remote and standoff sensing systems based on M-PEMS may include lidars, ladars, and hyperspectral imagers. All these systems will greatly benefit from the massive data fusion intrinsically performed by the optical systems of M-PEMS sensors. Such sensors may thus even provide the basis for very fast automated defense system.

2. PEM/FT SPECTROMETRY FUNDAMENTALS

2.1 UHS Spectral Modulation Using PEM-Based Interferometers

PEM/FT spectrometers are based on birefringence interferometers, which introduce a variable retardation between interfering waves separated by their mutually orthogonal directions of polarization. The retardation is proportional to the instantaneous birefringence of the modulator and can be varied in time in order to scan an interferogram. PEM-based FT spectrometers cover broad spectral ranges (UV to NIR with fused silica optics, and NIR to mid-IR with ZnSe optics). In its simplest implementation (Fig. 1), a birefringence interferometer consists of a birefringent modulator placed between two polarizers (Buican, 1985, 1990). The optical axes of the

Report Documentation Page

Form Approved
OMB No. 0704-0188

1. REPORT DATE	2. REPORT TYPE	3. DATES COVERED
01 NOV 2006	**N/A**	**-**

4. TITLE AND SUBTITLE	5a. CONTRACT NUMBER
Multivariate Pem/Ft Spectrometry: Intrinsic Data Fusion And Applications For Ied And Cb Defense	5b. GRANT NUMBER
	5c. PROGRAM ELEMENT NUMBER
6. AUTHOR(S)	5d. PROJECT NUMBER
	5e. TASK NUMBER
	5f. WORK UNIT NUMBER
7. PERFORMING ORGANIZATION NAME(S) AND ADDRESS(ES) **US Army RDECOM Edgewood Chemical Biological Center (ECBC) Aberdeen Proving Ground, MD 21010**	8. PERFORMING ORGANIZATION REPORT NUMBER
9. SPONSORING/MONITORING AGENCY NAME(S) AND ADDRESS(ES)	10. SPONSOR/MONITOR'S ACRONYM(S)
	11. SPONSOR/MONITOR'S REPORT NUMBER(S)

12. DISTRIBUTION/AVAILABILITY STATEMENT
Approved for public release, distribution unlimited

13. SUPPLEMENTARY NOTES
See also ADM002075., The original document contains color images.

14. ABSTRACT

15. SUBJECT TERMS

16. SECURITY CLASSIFICATION OF:			17. LIMITATION OF ABSTRACT	18. NUMBER OF PAGES	19a. NAME OF RESPONSIBLE PERSON
a. REPORT	b. ABSTRACT	c. THIS PAGE			
unclassified	**unclassified**	**unclassified**	**UU**	**8**	

Standard Form 298 (Rev. 8-98)
Prescribed by ANSI Std Z39-18

birefringent modulator are at 45^0 relative to the direction of the polarizers.

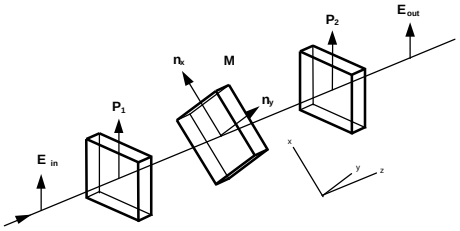

Fig. 1: The basic birefringence interferometer. E_{in}, E_{out}, input and output electric vectors; M, birefringence modulator; n_x, n_y, principal indices of refraction of the birefringence modulator and the corresponding optical axes; and P_1, P_2, polarizers and their optical axes.

The birefringence interferometer in Fig. 1 can be regarded as an optical frequency-dependent intensity modulator, with a spectral modulation function $M_{\Delta n}(\omega) = I_{out}(\omega)/I_{in}(\omega)$ controlled by the instantaneous birefringence $\Delta n = n_x - n_y$. The amplitude of the phase difference for interfering monochromatic waves of frequency ω is $\Phi = \gamma\omega$ [1], where the retardation amplitude $\gamma = \tau_{max}$ is the maximum time delay between the interfering waves. For a lossless interferometer, the modulation function is $M_\tau(\omega) = [1+\cos(\tau\omega)]/2$. For a birefringence interferometer using PEMs, the temporal retardation is given by $\tau(t) = \gamma\omega\sin(\omega_0 t)$, where ω_0 is the angular frequency of the PEM's mechanical oscillation, and the retardation amplitude is given by $\gamma = Bl/c$, where B is the birefringence amplitude, and l is the thickness of the birefringent modulator. Thus, for PEM-based birefringent interferometers, the spectral modulation function is

$$M(\omega,t) = I_{out}(\omega)/I_{in}(\omega) = \frac{1}{2}\left[1+\mathrm{b}(\gamma\omega,\omega_0 t)\right], \qquad (1)$$

where $\mathrm{b}(\Phi,\psi) = \cos(\Phi\sin\psi)$. The harmonic rather than linear time dependence of the interferogram phase for a PEM-based interferometer at first appears to be an inconvenience but in fact plays an essential role in active multivariate spectrometry.

2.2 Active PEM/FT Spectrometry

We developed the concept of multivariate PEM/FT spectrometry (Buican, 1993, 1995), in which both the illumination beam and the collected light pass through PEM-based interferometers (Fig. 2). In such a system, the chirped modulation of the illumination beam encodes a time origin for each half-period of the PEM, while also encoding the spectrum of the illumination beam. This information can subsequently be used in order to extract from the total collected intensity waveform (interferogram) the delays and delay distributions associated with each illumination wavelength. By also passing the collected light through a PEM-based interferometer, one can further encode into the interferogram the spectrum of the collected light. The latter can differ from the illumination spectrum if inelastic scattering and/or fluorescence are present.

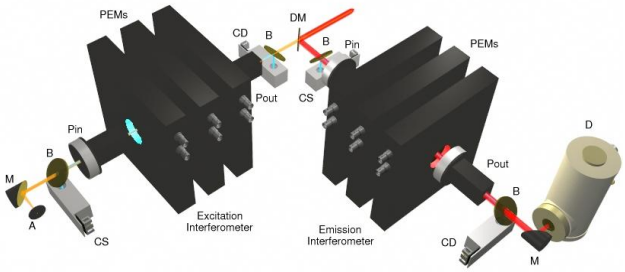

Fig. 2: Conceptual design of a trivariate PEM/FT spectrometer operating in the infrared. A, input aperture; B, beam splitter; CS, wavelength calibration source; CD, wavelength calibration detector; D, detector; DM, demultiplexer; M, off-center parabolic mirror; P_{in}, P_{out}, input and output polarizers; and PEMs, photoelastic modulators. The illumination/excitation beam is represented in yellow, while the collected/emitted light is represented in red.

The interferogram generated by the detector of a multivariate spectrometer is a linear transform of an intensity spectrum which itself is a function of three independent variables: the illumination frequency, the collection frequency, and the delay between illumination and collection. In a fluorescence microscope or flow cytometer (Fig. 3a), the only significant delays between the modulation of the illumination beam and that of the collected light are directly related to fluorescence lifetime and the interferogram generated by the dual PEM/FT spectrometer encodes a sampling of the FT of an intensity spectrum that that is simultaneously a function of excitation optical frequency, emission optical frequency, and fluorescence lifetime. In a lidar application (Fig. 3b), the propagation delays dominate and the multivariate spectrum involved is a function of excitation and emission optical frequencies, and of propagation time (range).

3. THEORY OF MULTIVARIATE SPECTROMETRY

3.1 The Direct Problem

The interferogram produced by a multivariate system such as the lidar in Fig. 3b is a linear transformation of a "trivariate spectrum", which is the distribution of collected[2] light intensity simultaneously over excitation frequency, emission frequency, and delay (range); we

[1] In the context of multivariate spectrometry, we choose the temporal rather than spatial versions of frequency and retardation because one of the variables of interest is the lifetime or propagation delay.

[2] The effect of the illumination and collection geometries and optics can be factored out to leave a "true" trivariate spectrum describing the intrinsic spatial and optical frequency properties of the target.

regard these as the natural spectral variables. If $S(\omega_x, \omega_m, \rho)$ is the trivariate spectrum in the natural

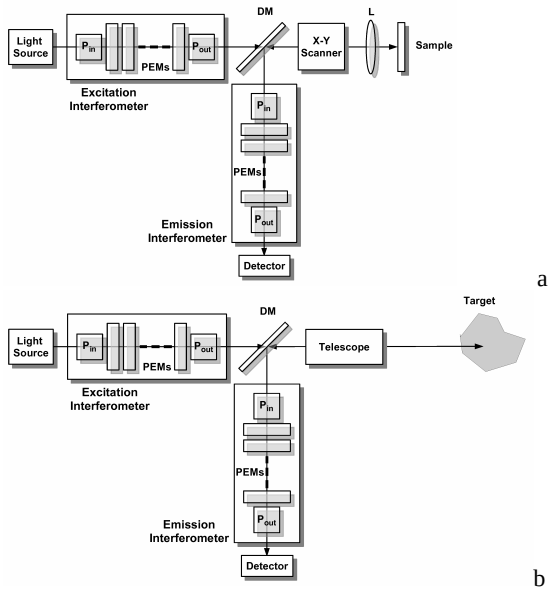

Fig. 3: Multivariate PEM/FT spectrometry. Simplified diagrams of two previously proposed instrumental configurations for multivariate spectrometry: a scanned multivariate hyperspectral fluorescence imager/microscope (a); and a multivariate fluorescence lidar (b). DM, dichroic mirror[3]; P_{in}, P_{out}, input and output polarizers; PEM, photoelastic modulator; L, lens (microscope objective optics).

variables, then the interferogram is given by the following integral transform:

$$I_d(t) = \alpha \int_0^\infty \int_0^\infty \int_0^\infty \left[1 + \mathrm{b}\left(\gamma_x \omega_x, \omega_{0x}(t-\rho) + \varphi_0\right)\right] \times \left[1 + \mathrm{b}\left(\gamma_m \omega_m, \omega_{0m} t\right)\right] S'(\omega_x, \omega_m, \rho)\, d\omega_x d\omega_m d\rho \quad , \qquad (2)$$

where $S'(\omega_x, \omega_m, \rho) = I_s(\omega_x) S(\omega_x, \omega_m, \rho) R(\omega_m)$ is the *effective* trivariate spectrum, with $I_s(\omega)$ the intensity spectrum of the light source and $R(\omega)$ the spectral responsivity of the detector; $\gamma_{x,m}$ are, respectively, the (temporal) retardation amplitudes of the excitation and emission interferometers; ω_{0x}, ω_{0m} are, respectively, the excitation and emission interferometers' angular frequencies of oscillation; φ_0 is the phase difference between the excitation and emission interferometers; and α is a system-dependent coefficient. This is the direct problem of trivariate PEM/FT spectrometry.

It is obvious from Eq. (2) that the transform mapping the trivariate spectrum to the interferogram is related to the cosine Fourier transform and will thus impose certain symmetry constraints on the system's spectral response. It is also obvious that it maps functions of three variables (the trivariate spectrum $S'(\omega_x, \omega_m, \rho)$) to functions of one variable (the interferogram) and therefore cannot be inverted in the strict sense of the word. Additionally, the retardation in PEM-based interferometers is a harmonic function of time. Finally, a dual interferometer system has five adjustable parameters[4] that affect the interferogram. Together, these factors seem to make multivariate PEM/FT interferograms nearly intractable. However, we show in the next subsection that there is an elegant geometric interpretation of the direct transform whereby the interferogram can be obtained by sampling, along a curved 3-D path, a function of three variables which itself is related to $S'(\omega_x, \omega_m, \rho)$ through a linear transform.

3.2 Separation of Sample and Instrument Descriptions

As the transform in Eq. 2 is linear, we will initially concern ourselves with a point spectrum in the space of natural coordinates, located at excitation and emission frequencies u_x , u_m , and delay v, and which describes a target that is excited only at an optical frequency u_x and which subsequently emits at the frequency u_m after a delay v,

$$S'(\omega_x, \omega_m, \rho) = \delta(\omega_x - u_x)\delta(\omega_m - u_m)\delta(\rho - v) \qquad (3)$$

(Fig. 4a). From Eq. (2), the interferogram for this point spectrum is

$$I_d(t) = \alpha\left[1 + \mathrm{b}\left(\gamma_x u_x, \omega_{0x}(t-v) + \varphi_0\right)\right]\left[1 + \mathrm{b}\left(\gamma_m u_m, \omega_{0m} t\right)\right]. \qquad (4)$$

If we change from the natural coordinates $\{\omega_x, \omega_m, \rho\}$ to the homogeneous ones $\{\omega_1, \omega_2, \omega_3\}$ in which the natural coordinates become cylindrical (Fig. 4b) by converting the delay coordinate ρ to a phase delay angle relative to the phase of the excitation interferometer,

$$\omega_1 = \omega_x \cos(\omega_{0x}\rho),\ \omega_2 = \omega_x \sin(\omega_{0x}\rho),\ \omega_3 = \omega_m\,, \qquad (5)$$

the original effective trivariate spectrum $S'(\omega_x, \omega_m, \rho)$ yields a new trivariate spectrum $S_h'(\omega_1, \omega_2, \omega_3)$ in the new, homogeneous, variables. We further construct a symmetrized spectrum S'_{hs} by adding to S'_h its reflections in the $\{\omega_1, \omega_2\}$ plane and the ω_3 axis[5] and finally we augment it to S'_{hsa} by adding projections onto the $\{\omega_1, \omega_2\}$ plane, the ω_3 axis, and the origin[6] (Fig. 4b).

A 3D Fourier transform $\mathscr{F}_3$ of the new spectrum S'_{hsa} yields a trivariate "interferogram" $I_{d,3} = \mathscr{F}_3 S'_{hsa}$, which, because of the symmetry properties of this

[3] A dichroic mirror is used in fluorescence applications to separate the emission and excitation wavelengths. For lidar applications in which backscattered light is important, a duplexer mirror will be used instead.

[4] Two retardation amplitudes; two scanning frequencies; and one relative phase.

[5] The symmetries added to the trivariate spectrum are a generalization of the inversion symmetry in standard FT spectrometry.

[6] The projections added to the trivariate spectrum correspond to the effects of the d.c. terms in the interferogram of Eq. 2.

spectrum, is a real function of three time-like variables (temporal retardations), $I_{d,3}(\underline{\tau})$, where $\underline{\tau} = (\tau_1, \tau_2, \tau_3)$ is a 3D

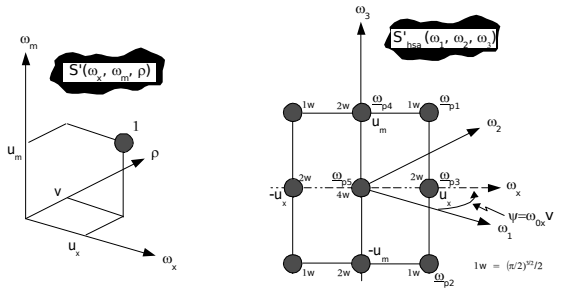

Fig. 4: Trivariate point spectrum in natural coordinates (a) and homogeneous frequency coordinates (b). The point spectrum in (b) has been symmetrized and augmented. u_m, u_x, v are, respectively, the emission and excitation optical frequencies, and the delay between excitation and emission for the trivariate point spectrum; w, unit of weight for the point distributions in space of homogeneous frequency coordinates; ψ, angular coordinate; $\underline{\omega}_{p1,\ldots5}$, position vectors in the space of homogeneous frequency coordinates for the various point distributions; ω_{0x}, mechanical oscillation frequency of the excitation PEM-based interferometer.

"time" vector. For the symmetrized and augmented point spectrum in Fig. 4b, the resulting 3D interferogram is

$$I_{d,3}(\underline{\tau}) = \beta[2\cos(\underline{\omega}_{p3}^T\underline{\tau}) + 2\cos(\underline{\omega}_{p4}^T\underline{\tau}) + 2\cos(\underline{\omega}_{p5}^T\underline{\tau}) + \cos(\underline{\omega}_{p1}^T\underline{\tau}) + \cos(\underline{\omega}_{p2}^T\underline{\tau})] \quad (6)$$

where β is a constant coefficient and the frequency vectors correspond to the positions shown in Fig. 4b. This is the "trivariate" interferogram, a real function over the space of 3D time vectors conjugate to the frequency vectors defined in Eq. (5). It is the sampling of this trivariate interferogram along a path parametrized by the actual time, $p = \{\underline{\tau}(t)\}$, that results in the interferogram generated by the detector, $I_d(t) = I_{d,3}(\underline{\tau}(t))$. For the system that generates the interferogram given by Eq. (4), the sampling path can be shown to be

$$\underline{\tau}(t) = \begin{bmatrix} \tau_1(t) \\ \tau_2(t) \\ \tau_3(t) \end{bmatrix} = \begin{bmatrix} \gamma_x \sin(\omega_{0x}t + \varphi_{0x}) \\ -\gamma_x \cos(\omega_{0x}t + \varphi_{0x}) \\ \gamma_m \sin(\omega_{0m}t) \end{bmatrix}. \quad (7)$$

As discussed in subsection 3.3, this is a Lissajous figure on a cylindrical surface. The time-dependent intensity resulting from the sampling of the trivariate interferogram in Eq. (6) along the path in Eq. (7) can be obtained by substituting in the former the time vector from the latter. The result can be shown to be the expected 1D time-dependent interferogram given by Eq. (4) for the trivariate point spectrum in Eq. (3).

It is important to notice at this point that the 3D interferogram, exemplified for the case of a point trivariate spectrum by Eq. (6), is independent of instrument parameters and exclusively describes the trivariate spectral properties of the sample/target. Because of the linear nature of the system, the same will be true for any arbitrary superposition of point spectra, and, thus, for arbitrary trivariate spectra. On the other hand, the sampling path given by Eq. (7) only depends on the instrument's parameters, such as the retardation amplitudes of the two PEM-based interferometers, their mechanical oscillation frequency, and their relative phase. Then, the actual 1D detector interferogram for any trivariate spectrum can be obtained by the same process of sampling the corresponding trivariate interferogram along the instrument-determined sampling path of Eq. (7).

Thus, while the multivariate interferogram is a description of the complex spectral properties of the sample, the geometry of the curved path is exclusively determined by the instrument's operating parameters and scanning characteristics. The two domains are reunited by sampling the multivariate interferogram along the instrumental path, which results in the actual time-dependent interferogram as generated by the detector. Resolving the complex trivariate spectrometry problem into a straightforward 3D FT and the geometry of the sampling path conveniently separates, conceptually and computationally, the spectral properties of the sample from the properties of the instrument.

This interpretation also exposes the way in which multivariate PEM/FT spectrometry is a direct generalization of standard FT spectrometry. Indeed, in standard FT spectrometry, the detector signal is a function of retardation, from which the actual interferogram signal is derived by scanning the retardation as a function of time. In the multivariate case, the detector signal is still a function of retardation, which is now a 3D vector, and the detector signal is again obtained by scanning the 3D retardation as a function of actual time, i. e., along a path in 3D space.

By applying an inverse 3D FT transform to both the trivariate interferogram and the sampling path results, respectively, in the (symmetrized and augmented) trivariate spectrum S'_{hsa} on the one hand, and the system's point response function on the other. This is the 3D frequency space equivalent of the separation of the problem into sample and instrument specific parts, with a convolution of the spectrum and point response function as the equivalent of the sampling along a path in the space of time-like coordinates.

3.3 Geometry of Interferogram Sampling

The trivariate interferogram, which is a function of three time-like variables, cannot be arbitrarily sampled. However, the temporal evolution of the phases of the two interferometers results in a 1D sampling path in the space of these three time-like variables. When sampled in this way, the trivariate interferogram yields information that

can be used to reconstruct, in a unitary and homogeneous way, the original trivariate spectrum[7].

The sampling path given by Eq. 7 is a Lissajous figure (Bogle et al, 1994) on the surface of a cylinder centered at the origin; with its axis parallel to the τ_3 axis and spanning the interval $\tau_3 \in [-\gamma_m, \gamma_m]$; and of radius γ_x (Fig. 5). We call this the sampling cylinder. The origin of

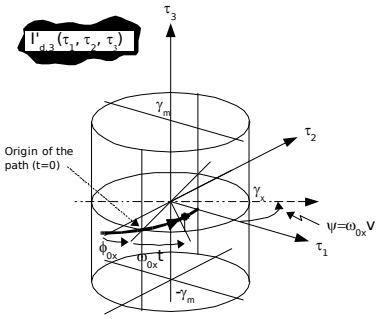

Fig. 5: Sampling path for trivariate interferograms. (See the text for definitions of the various parameters.)

the angular coordinate in the $\{\tau_1, \tau_2\}$ plane is at $-\pi/2$, and the origin of the path is rotated by φ_{0x} relative to it. The sampling path is a closed curve if the ratio of the PEM-based interferometer frequencies, ω_{0x}/ω_{0m}, is a rational number. In the simplest case, the two frequencies are equal and the path is an ellipse with its plane rotated by the initial phase φ_{0x}. Several closed paths with zero initial phases are shown in the first column of Fig. 6. It is obvious that, by manipulating the ratio of the two PEM frequencies, one can achieve as fine a scanning of the sampling cylinder as desired, but at the cost of increased scanning time. Indeed, if $\omega_{0x}/\omega_{0m} = n/m$, where *m* and *n* are coprime, then *m* gives the number of full oscillations of the sampling path along the τ_3 axis, while *n* is the number of full circles in the $\{\tau_1, \tau_2\}$ plane, for one full period of the closed sampling path. Thus, the time required to travel the full sampling path, and thus generate a full interferogram and acquire all the accessible spectral information, is $T_{scan} = 2m\pi/\omega_{0m}$ and increases linearly with the density of the coverage of the sampling cylinder by the sampling path.

In the limit of infinite scanning time, the sampling path passes through every point of the sampling cylinder. This ideal case represents the best one can do in terms of sampling the trivariate interferogram for given retardation amplitudes γ_x, γ_m. The ideal spectral point response function can be easily derived as the inverse 3D FT of the sampling cylinder, and is given by

$$H_{\gamma_x,\gamma_m,\infty}(\underline{\omega}) = \kappa\, \mathrm{J}_0(\gamma_x\sqrt{\omega_1^2+\omega_2^2})\,\mathrm{sinc}(\gamma_m\omega_3)\,, \qquad (8)$$

where κ is a constant. This ideal spectral point response function is illustrated in the last row of Fig. 6, where one can notice that the response spreads out more in the excitation/delay plane $\{\omega_1, \omega_2\}$ than along the emission axis ω_3, as the former is governed by the Bessel function J_0, while the later by a sinc function. One can also see that, for $n \neq m$, the sampling path spectral response functions quickly approach that for the sampling cylinder itself. Indeed, even for n/m=6/5, the spectral response function in a plane containing the emission frequency axis differs from the ideal one mostly in the higher-frequency diagonal regions of the plots which are associated with the angular periodicity of the path on the cylinder. At n/m=21/20, the angular period of the path has already decreased to the point where these diagonal contributions have moved to even higher frequencies and out of the plots.

4. DATA FUSION AND POSTPROCESSING

4.1 Intrinsic Data Fusion

Data fusion—the process of combining and representing disparate data in a correlated and homogeneous form that can be effectively and efficiently processed by discrimination and identification algorithms—is a major requirement for any realistic CB or IED warning system. It allows small but specific changes in individual detector signals to be extracted from the noise of the environment by identifying specific correlations that are absent from the stronger but nonspecific noise. In the M-PEMS context, we refer to this as the Correlated Multivariate Advantage.

Conventional data fusion is performed numerically on the signals collected from a multitude of separate sensors and may require sophisticated software and considerable data processing and storage resources. M-PEMS fuses data for three important optical spectral variables, namely excitation and emission frequency and emission delay/lifetime by means of the massively parallel processing power of its optical system, and generates one signal, the interferogram, that encodes the fused data. Thus, the task of digital postprocessing is now reduced to discrimination and identification. While nontrivial, this task can be relatively easily performed in compact, high-performance hardware that can be embedded into a mobile and even portable detection system.

A multivariate PEM/FT spectrometer functions as a massively parallel optical computer which computes in parallel at all excitation and emission frequencies, and time delays. Of course, a standard FT spectrometer also optically computes in real-time and in parallel the (cosine) FT of a spectrum, but a multivariate PEM/FT takes this massively parallel computation to a new level by carrying out at full speed a 3D FT and a 1D sampling.

[7] Within the resolution allowed by the spectral response function corresponding to the instrument's operating parameters.

The three types of data optically processed and fused by an M-PEMS are brought together in the homogeneous and correlated representation of the trivariate spectrum and, through an optically computed 3D FT, in

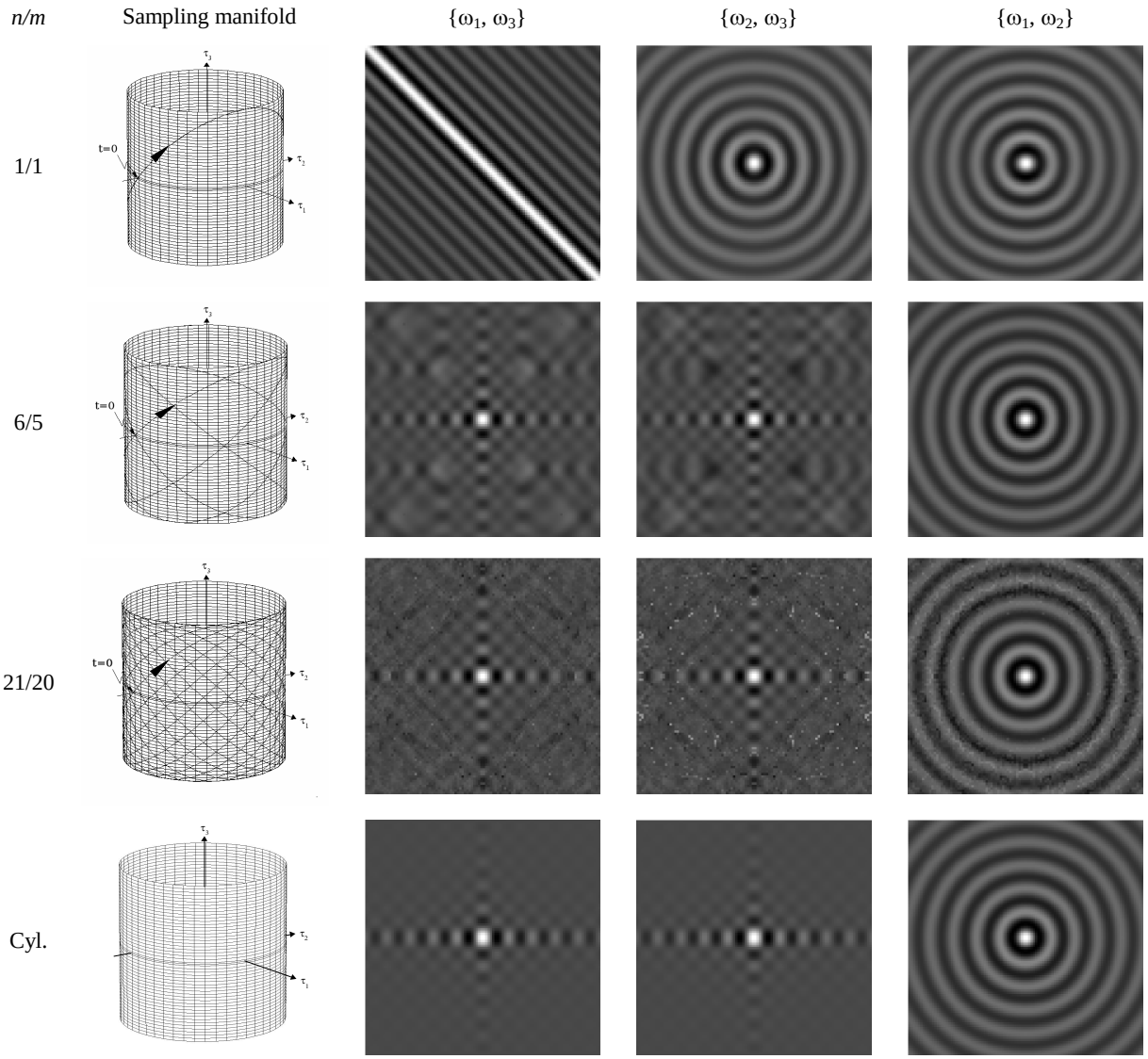

Fig. 6: Trivariate spectral response functions for various sampling paths. The first column shows various sampling manifolds, including both sampling paths ($\omega_{0x} / \omega_{0m} = n/m$ values of 1/1, 6/5, and 21/20) and, in the limit, the full sampling cylinder. The other three columns show three orthogonal sections (in the planes $\{\omega_1, \omega_3\}, \{\omega_2, \omega_3\}, \{\omega_1, \omega_2\}$) through the corresponding response functions. The horizontal and vertical axes of the response function plots correspond respectively to excitation/delay and emission frequencies ($\omega_x = (\omega_1^2 + \omega_2^2)^{1/2}$, $\omega_m = \omega_3$.). These plots extend to approximately 10 resolution widths from the origin, which is at the center of each plot. Similar results are obtained for n<m.

the trivariate interferogram. The actual data fusion process, which generates a single signal that encodes in a correlated way the three types of data, consists of sampling the trivariate interferogram along a particular sampling path. The characteristics of the fusion process, i. e., the way in which the contributions of certain spectral details are enhanced relative to others, are controlled through the geometry of the sampling path and thus, eventually, through the adjustable instrument parameters. Thus, the geometric interpretation of the direct transform of trivariate spectrometry becomes the basis for programming a multivariate M-PEMS as a data fusion optical processor.

Furthermore, the data fusion process performed by the M-PEMS can be made to adapt to the actual data so as to maximize its discrimination and identification power. This can be achieved by controlling the instrument

parameters, and thus the sampling path, through a closed loop driven by an external data postprocessor.

4.2 External Data Postprocessing for Discrimination and Identification

With suitable data acquisition and processing electronics, PEM/FT spectrometers can acquire and linearly extract spectral parameters during the very scanning of the interferogram, with additional dead times of less than 1 μs. This is made possible by the use of dedicated real-time linear parallel processors for spectral deconvolution, the first of which was developed by us in the mid-80s (Buican, 1985).

A linear processing stage can greatly reduce data dimensionality at the full speed of data acquisition. A second, nonlinear stage in a data processing pipeline can perform high-performance discrimination and identification tasks. Our work on supervised and unsupervised neural network learning may provide an integrated neural network architecture for spectral identification (Carrieri, 1999) offering distributed analytic capabilities to characterize known threats by type and concentration. Such backward-error propagation and self-organization mapping analytic neural network engines will incorporate technology capable of learning to characterize IEDs and unknown CB substances in the specific M-PEMS instrumentation, data acquisition, preprocessing, and software context.

5. PRELIMINARY DESIGN CONSIDERATIONS

M-PEMS requires accurate and stable control of the geometry of the sampling path and thus of the interferometers' retardation amplitudes and oscillation frequencies, as well as of their relative phase. While commercial PEMs are still essentially free running oscillators whose frequency drifts uncontrollably with temperature and amplitude, our work on driving and controlling PEMs and PEM stacks at high retardation amplitudes (Buican and Carrieri, 2004; Buican, 2005, 2006) has eliminated this problem.

We showed (Buican, 1997) that spectral resolutions of 10 cm^{-1} and better can be achieved in the infrared with stacked PEMs. The time (delay) resolution can be estimated from Equations (5) and (8) as being $\delta\rho \approx \delta\omega_x / (\omega_{0x}\omega_x)$ and thus dependent on the excitation optical frequency, as well as on the frequency of the mechanical oscillation of the excitation PEM-based interferometer. For a spectral resolution of 10 cm^{-1}, an excitation wavelength of 1 μm, and a PEM frequency of 30 kHz, the resulting delay resolution is of the order of 5 ns. In a lidar application, this corresponds to a range resolution of 0.75 m. It should be noted that superresolution can be achieved when the number of basis spectra is limited to those associated, for example, with known threats.

We also showed in subsection 3.3 that the duration of a full scan of the sampling path is proportional to the density of the coverage of the sampling cylinder by the path. Preliminary results suggest that fairly low values of the scanning parameters *m* and *n* such as *n/m*=6/5 result in response functions that are likely to suffice in many important applications. With an emission interferometer running at 30 kHz, this results in the acquisition of 6,000 double interferograms per second and a trivariate spectrum-based analysis roughly every 84 μs.

A multivariate PEM/FT spectrometer can cover the spectral region from the UV to near IR with one set of optics (fused silica), and from the red to 12 μm with another (ZnSe). Thus, the advantages of intrinsic multivariate data fusion are complemented in PEM/FT spectrometers by extended spectral range, which makes possible discrimination and identification based simultaneously on a very wide range of mechanisms of interaction between targets and optical radiation.

6. APPLICATIONS FOR IED AND CB DEFENSE

Multivariate PEM/FT spectrometry is potentially the enabling technology for fast multivariate biological and chemical detection and mapping. We make this claim because even in its most basic implementation an M-PEMS instrument offers a more complete description of the interactions between light and sample/target than any other single instrument. Indeed, in basic M-PEMS, the target's interactions with light are represented by a trivariate spectrum in which spectral properties in terms of excitation, emission, and delay/lifetime are depicted in a correlated way. When used for discrimination based on trivariate spectral signatures, the interferogram signal carries encoded information allowing for discrimination on the basis of spectral differences in this 3D space of spectral variables. In other words, the same M-PEMS system can not only simultaneously discriminate, for example, between different fluorescent species or between elastic scatterers at different ranges, but can also simultaneously resolve fluorescence from inelastic scattering, while extracting some range information as well.

The basic M-PEMS technology (i) provides active spectral analysis, without having to rely on external and uncontrollable light sources; (ii) is broadband, with only two optical materials covering VUV to NIR and NIR to 12 μm, and thus covering electronic, vibrational, and rotational transitions and their interactions; and (iii) operates at ultra-high speeds, with an interferogram being scanned, acquired, and processed, depending on instrument configuration, in an interval from several microseconds to milliseconds—it can thus deal with fast changing targets in single-shot mode, and potentially with

ultrafast light sources and target events in a repetitive excitation mode.

To these interesting capabilities one can add the eminently feasible concept of an ultra-broadband M-PEMS instrument covering essentially the full spectral range from the UV to 12 μm. With suitable light sources, such an instrument could simultaneously analyze (i) the UV-VIS LIBS fluorescence of ions and neutral species in the plasma plume created by an ultra-short laser pulse; (ii) the possible fluorescence of molecular fragments at the periphery of the ablation zone; and (iii) the IR emission of the same molecular fragments. Such a system would complement the abundant but potentially ambiguous LIBS data with the much more specific molecular IR spectral information. Such a system would likely be useful in identifying specific surface contaminants associated with, for example, improvised explosive devices (IED).

The extension of multivariate spectrometry to include the spectral dependence of changes in polarization resulting from the interaction between target and the modulated illumination beam promises to further increase the discrimination and identification capabilities of multivariate spectrometry. Indeed, work done on differential-absorption Mueller matrix spectroscopy (DIAMMS) (Carrieri et al., 1998; Carrieri, 1999) indicates that this may well be the case.

If this potential is realized, M-PEMS can become the technique of choice for many important applications aimed at protecting the warfighter on the battlefield and the civilian population in the homeland. Potential applications of M-PEMS range from early detection and reliable identification of biological agents and IEDs, to compact and fast detectors built into smart munitions that could recognize contaminated targets, as well as to fast automated CB and IED defense systems. The civilian population would also benefit from the widespread use of such highly sensitive and reliable detectors of biological agents, which could be used to monitor in real time large public spaces such as airports and supermarkets, or confined spaces such as HVAC air ducts.

CONCLUSIONS

We believe that active multivariate PEM/FT spectrometry has the potential to become the enabling technology for fast, sensitive, and reliable optical detection and identification of specific chemical and biological agents and contaminants. We also believe that active, correlated, multivariate spectrometry is superior to other optical techniques in that it offers comprehensive fused optical data in a form that is suitable for the highly efficient and reliable detection and identification of threats.

By providing a comprehensive correlated description of optical properties that can only be richer in information than the more common uncorrelated descriptions, M-PEMS may open a new window on the optical properties of complex biological materials. Independently of any security applications, M-PEMS thus has the potential to become the spectrometric technique of choice for the study of dynamic biological and chemical systems.

REFERENCES

Bogle, M.G.V., Hearst, J.E., Jones, V.F.R., Stoilov, L., 1994: Lissajous Knots, *J. Knot Theory and Its Ramifications* 3, 121-140.

Buican, T.N., 1985: Fourier Transform Flow Cytometry – The Interferometric Analysis of Emission Spectra from Individual Cells. Proc. 11th Intl. Conf. of Analytical Cytology, Hilton Head, SC, Intl. Soc. Analyt. Cytology.

Buican, T. N., 1990: Real-Time Fourier Transform Spectrometry for Fluorescence Imaging and Flow Cytometry. Proc. SPIE Symposium on Bioimaging and Two-Dimensional Spectroscopy, Los Angeles, CA, SPIE, 126-133.

Buican, T.N., 1993: Apparatus and Method for Measuring Fluorescence Intensities at a Plurality of Wavelengths and Lifetimes, US Patent No. 5,208,651.

Buican, T.N., 1995: Trivariate Spectral Analysis: An Integrated Approach to Excitation, Emission and Lifetime Spectral Analysis. SPIE Biomedical Optics Symposium, San Jose, California.

Buican, T.N., 1997: Feasibility Study for the Development of a High-Speed Fourier Transform Infrared (FTIR) Photoelastic Modulator (PEM) Based Spectrometer. Tech. Report to ERDEC, TCN Number 95-035, BTI, Albuquerque, NM.

Buican, T.N., 2005: Controlling Resonant Photoelastic Modulators. US Patent No. 6,970,271.

Buican, T.N., 2006: Birefringence Interferometers for Ultra-High-Speed FT Spectrometry and Hyperspectral Imaging: I. Dynamic Model of the Resonant Photoelastic Modulator, In press, *Vibrational Spectroscopy*, proofs available online at http://dx.doi.org/10.1016/j.vibspec.2006.04.011.

Buican, T.N. and Carrieri, A.H., 2004: Ultra-High Speed Solid-State FTIR Spectroscopy and Applications for Chemical Defense. 24th Army Science Conference Proceedings, http://handle.dtic.mil/100.2/ada431953.

Carrieri, A.H., 1999: Neural network pattern recognition by means of differential-absorption Mueller matrix spectroscopy, *Applied Optics*, 38, 3759-3766.

Carrieri, A.H., Bottiger, J.R., Owens, D.J., Roese, E.S., 1998: Differential-absorption Mueller matrix spectroscopy and the infrared detection of crystalline organics, *Applied Optics* 37, 6550-6557.

Stann, B.L., Ruff, W.C., Sztankay, Z.S., 1996: Intensity-modulated diode laser radar using frequency-modulation/continuous-wave ranging techniques, *Opt. Eng*., 35, 3270-3278.